Attenuation of progressive surface gravity waves by floating spheres

Calvert, Ross; Mol, Jessamy; Sutherland, Bruce R.; van den Bremer, Ton S.

DOI
10.1038/s41598-025-86142-4

Publication date
2025

Document Version
Final published version

Published in
Scientific Reports

scientific reports

Check for updates

OPEN

Attenuation of progressive surface gravity waves by floating spheres

Ross Calvert[1,2], Jessamy Mol[1], Bruce R. Sutherland[3,4] & Ton S. van den Bremer[1]✉

Laboratory experiments were performed to investigate the attenuation of progressive deep-water waves by a mono-layer of loose- and close-packed floating spheres. We measured the decay distance of waves having different incident wave frequency and steepness. The attenuation of waves was strong if the surface concentration of particles was close-packed, with the decay distance being shorter for incident waves with higher frequency and steepness. The amplitude of the highest-frequency (2.0 Hz) and largest amplitude incident waves (with steepness 0.25) decayed by half over a distance of approximately 3 wavelengths. Theoretical models used previously in the study of surface wave damping by sea ice do not capture correctly the physics of wave attenuation by floating spheres. We developed a new theory that estimates the influence upon wave attenuation of turbulent dissipation resulting from oscillatory flow under a close-packing of spheres. This theory predicts that the wave amplitude decays as a power law, and gives a correct order-of-magnitude estimate of the observed decay distance. We explore the potential implications of these findings for the attenuation of progressive waves by (pancake) sea ice and for the indirect detection of marine plastic pollution from space.

It is well established that surface waves can be damped by oil slicks[1], foam[2,3] and sea ice[4]. The rate at which sea ice damps waves is of particular interest because the waves can mechanically contribute to the break-up of ice in polar regions, where ice is retreating and thinning in a warming climate. Consequently, of all the phenomena that can lead to damping of surface waves, sea ice has probably received the most attention.

The amplitude decay of waves passing under ice has been investigated experimentally using wave flumes[5–7], observed in field measurements[8,9], and different types of theories have been proposed to model it. In principle, the observed amplitude decay can be due to a combination of two processes, scattering and dissipation, where scattering only redistributes energy but does not eliminate it. Which of these two processes is dominant depends on the composition of the sea ice and the properties of the wave field, and most operational models of wave evolution under sea ice include models for both processes.[4]

Interaction between waves and individual ice floes of characteristic sizes comparable to the wavelength results in reflection of a proportion of the incident wave energy, dissipation of part of it, and transmission of the remainder. In this regime, theoretical and numerical methods based on thin-plate theory for individual floes and potential flow have been compared to experiments[10] and can be combined to derive the properties of a large field of floes[5,11].

When the ice floes are much smaller than the wavelength, as is the case with pancake ice, waves are typically assumed to decay primarily as a result of viscous losses, and the sea ice is modeled as a continuous medium. Many continuous-medium models suggest an exponential decay rate[12], such as theories that assume that the surface can be treated like an enhanced viscous fluid[13,14] or a viscoelastic sheet[15,16]. Shen and Squire[17] modeled pancake ice and derived a power law for the attenuation by sea ice due to collisions of pancake ice. Squire[18] created a more general model for attenuation using a generic ordinary differential equation with a solution that can be exponential or power law depending on a chosen variable.

Sutherland & Balmforth[19] examined the temporal damping of sloshing waves in a rectangular tank by a close-packing of floating spheres. While wave-damping by a single layer of spheres was found to be exponential in time, they found that the waves became fully damped in a finite time, following a power law, if the spheres were two or more layers deep. Gurusamy et al[20] carried out similar experiments on sloshing waves damped by spheres. However, they did not examine the overall (spectral) decay rates, instead focusing on how the presence of floating spheres altered the decay of the first and third modes. They showed that the decay rate increased with frequency as the wave frequency squared, although they only had three data points. In Alberello et al[6], ice cubes at different concentrations were used to model pancake ice, and wave energy dissipation was measured to be

[1]Faculty of Civil Engineering and Geosciences, Delft University of Technology, 2628 CD Delft, The Netherlands. [2]School of Engineering, University of Edinburgh, Edinburgh EH9 3FB, UK. [3]Department of Physics, University of Alberta, Edmonton, AB T6G 2E1, Canada. [4]Department of Earth and Atmospheric Sciences, University of Alberta, Edmonton, AB T6G 2E3, Canada. ✉email: t.s.vandenbremer@tudelft.nl

the highest at high frequencies. Sun et al[21] examined the effect of floating particles and surfactants on the mean-square surface slope of wind- and wavemaker-generated irregular waves in a flume tank. Using 0.5 or 0.8 cm plastic particles and irregular waves with a peak frequency of 1.25 Hz, they found that 10% by area particle concentrations produced a 10% decrease in the mean-square slope compared to clean-water results, although surfactants had a more significant effect at lower concentrations.

Here, we study the spatial damping of progressive waves by a single layer of floating spheres. Unlike Sun et al,[21] we focus on measuring the decay distance of waves passing below near close-packed particle concentrations. We begin by presenting the set-up, analysis and results of laboratory experiments, which show rapid attenuation of sufficiently high-frequency incident waves. In developing a theoretical prediction for these results, we argue that existing theories used for wave-damping by floating ice do not capture the essential physics of wave motion below spherical particles by neglecting the influence of their effective collective roughness. We then develop a new semi-empirical theory that accounts for wave attenuation due to turbulence at the base of the floating spheres. We conclude by summarizing results and considering potential applications to wave-damping by (pancake) sea ice and possible detection of floating marine plastic pollution by satellites.

Laboratory experiments

Here, we describe the set-up of the experiments and the analysis tools used to measure the evolution of the waves as they pass below floating particles. We go on to present measurements of the decay distance of the wave amplitude.

Experiment set-up

Experiments were performed in a 35 m long, 0.5 m wide flume tank filled to a depth $h = 0.7$ m with fresh water. As illustrated in Fig. 1, a programmable wavemaker at the left end of the tank was designed to create sinusoidal surface waves with specified frequency and amplitude. A sloping beach located at the right end of the tank was shown to eliminate the reflection of incident waves effectively (we note that due to the damping of waves by the plastic particles and the timing of the measurements, reflections from the beach are not an important concern).

The incident wave frequency ranged from $f = 1.0$ to 2.0 Hz ($\omega = 6.28$ to 12.6 rad /s) with respective wavelengths ranging from $\lambda = 1.56$ m to 0.39 m. The corresponding wavenumbers, which ranged from $k = 4.03$ rad /m to 16.11 rad /m , were sufficiently large compared to h^{-1} that the waves could be treated as deep-water waves, having negligible motion at the bottom of the tank. The wave amplitude, a_0, was set depending upon the wave frequency (hence wavenumber) so that the wave steepness, $\epsilon \equiv ka_0$, had values of 0.10, 0.15, 0.20 and 0.25.

Control experiments were performed without floating particles in order to examine the wave evolution even in the absence of floating particles, particularly in the case of moderately large amplitude waves. Experiments with particles used a large number of $D = 20$ mm-diameter yellow polypropylene spheres. These spheres had density $\rho_p = 0.92$ g /cm^3, moderately smaller than that of the fresh water in the tank so that the spheres floated with 1/6 of the diameter extending above the surface.

Before the start of an experiment with particles, a front-barrier spanning the width of the tank across its surface was placed 11 m from the wavemaker and a second barrier was placed 7 m further downstream. In most experiments, enough polypropylene spheres were added between these barriers to create a single layer of close-packed spheres. Such experiments are said to have an area concentration of 100%. Fewer spheres were added in subsequent experiments to reduce the concentration. The rear and front barriers were then removed, and the wavemaker started shortly thereafter.

After the barriers were removed, the particles near the front and back of the pack slowly drifted upstream and downstream, respectively, at around a few millimeters per second. The time of removal of the front-barrier to the time of arrival of the first waves from the wavemaker was about 15 s. In this time, the front ~ 0.5 m of floating particles were no longer closely packed. This initial spreading of the particle fronts had insignificant

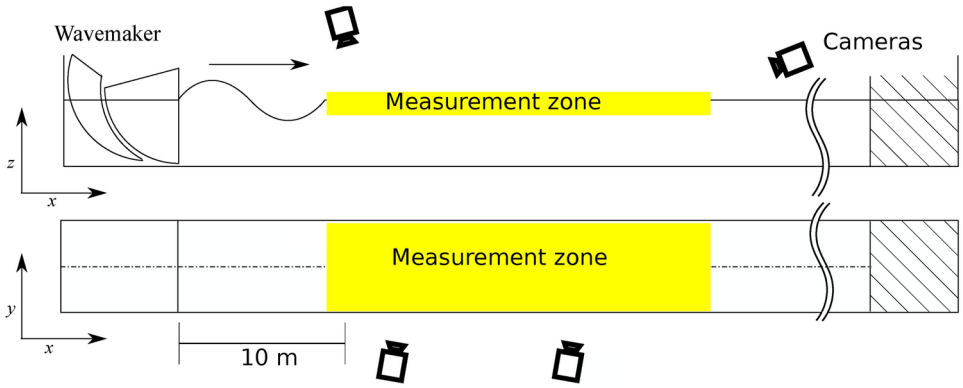

Figure 1. Side view (top image) and top view (bottom image) of the set-up of the experimental flume tank with top and side camera positions indicated. The measurement zone was situated between 10 m and 20 m from the wave maker.

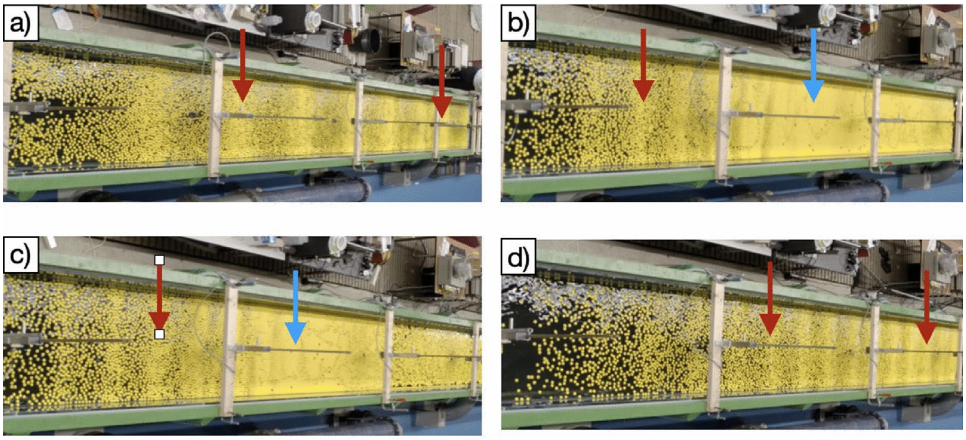

Figure 2. Snapshots taken from the overhead camera looking down the length of the tank for four experiments in quasi-steady state, all with incident wave steepness $\epsilon = 0.20$. In (**a**–**c**) there is an initial close-packed (100%) concentration of particles and the wave frequency is (**a**) $f = 1.2$ Hz, (**b**) $f = 1.6$ Hz and (**c**) $f = 2.0$ Hz. In (**d**) the initial area concentration is 71% and the wave frequency is 1.8 Hz. Red arrows in point to selected bands of brighter yellow regions where waves consolidate particles at wave crests. The blue arrows in (**b**,**c**) point to where the particles are close-packed and the surface has become undisturbed by waves that have fully attenuated.

Figure 3. Image from a side-camera of the experiment shown in Fig. 2c) illustrating that the close-packed spheres attenuate the rightward propagating incident wave to near zero amplitude over a horizontal distance of 3.5 m.

influence upon the later time wave-particle interactions as a consequence of waves acting to compact and thus evenly distribute the field of particles.

The wave evolution below near close-packed spheres was strongly influenced by the incident wave frequency, amplitude and the initial concentration of floating particles, as illustrated in Fig. 2. At a relatively low frequency, waves propagated all the way through the pack of floating spheres with negligible damping. This is evident, for example, in an experiment with $f = 1.2$ Hz shown in Fig. 2a in which the successive bands of brighter and darker yellow regions correspond to the alternate consolidation and spreading of particles between wave crests and troughs, respectively. For sufficiently high incident wave frequencies and amplitudes, we found that near close-packed particles efficiently damp the waves. This is shown in Fig. 2b,c, for experiments with $f = 1.6$ Hz and 2.0 Hz, respectively. The attenuation of waves by the particles resulted in a near-surface convergent drift that maintained the spheres in a close-packing configuration. The close-packing further enhanced wave attenuation such that the waves attenuated to zero amplitude in a finite distance. This is clear from side-view images of such experiments, as shown for example in Fig. 3. In experiments for which the initial concentration of particles was not close-packed, waves passed through the particles with reduced attenuation even at large frequency (Fig. 2d).

Experiment analyses

Analyses were performed on the waves after they reached quasi-steady state. The start of this analysis was determined from data from the leading wave gauge, upstream of the particle pack. The gauge recorded the time when the first wave crest reached the instrument. The start time of the analysis (denoted $t = 0$) was then taken to be this time plus the time, L_m/c_g, for wave energy to cross the measurement zone with length L_m moving at the group velocity c_g.

In some experiments for which wave attenuation was relatively weak, the decay of amplitude with downstream distance was measured by 10 resistance-type wave gauges used to record surface displacement at a rate of 100 Hz. Eight of these wave gauges where situated at mid-span of the tank, spaced over the 10 m observation window that was initially covered by floating particles. Of the other two gauges, one was located upstream and the other far downstream of the particle pack. In experiments for which wave attenuation was strong, the amplitude decay was measured by two Go-Pro cameras, together capturing a 3.5 m wide side view of the tank between 11.38 m

and 14.58 m from the wavemaker. Each camera had a resolution of 2704×1502 pixels, recording at 24 frames per second. An image captured by one of these cameras is shown in Fig. 3. Measurements of amplitude displacement were performed using MATLAB. Twelve points spanning the field of view of each camera were used to construct world-map co-ordinates, which related pixel locations to horizontal and vertical co-ordinates at the side of the tank wall facing each camera. Vertical time series of the surface position were constructed by extracting vertical slices at a range of horizontal positions and stacking these in time. Between the two cameras, the vertical slices were taken every 25 cm between 1138 cm and 1488 cm from the wavemaker. From one of these time series, an estimate of the vertical location in time of the wave surface was determined by detecting the highest yellow pixel (associated with the plastic spheres) at each time. This method in effect determined the surface displacement at the side of the tank facing the cameras. It was clear that the motion of the spheres against the tank sidewalls was the same as the motion of spheres in the tank interior (i.e., there were negligible frictional or viscous boundary effects at the walls). The surface displacement in time at a given horizontal location was then found by measuring the pixel displacement relative to the initial time before the waves arrived, and using the worldmap to convert this to vertical displacement to an accuracy of 0.3 mm and a time resolution of 0.04 s.

From surface displacement measurements from the wave gauges and cameras, we determined the amplitude, A, of the waves. First, we constructed the root-mean-square (rms) time-average over a sliding window having a duration of 5 wave periods. Because the rms average of a sinusoidal signal is its amplitude divided by $\sqrt{2}$, we multiplied the average by $\sqrt{2}$ to cast the result in terms of amplitude. An example of this analysis is shown in Fig. 4. The camera measurements of surface displacement and amplitude were validated against wave-gauge measurements as shown, for example, in Fig. 4. In general, the wave amplitude derived from the cameras agreed to within 5% of the wave gauge amplitude measurements. The error caused by not taking into acount the effect of higher-order harmonics[22] is small and can be neglected (see Tab. 1 in the Supplementary Information).

By applying this analysis to all the measurements from the wave gauges and vertical time series from the cameras, we constructed the spatio-temporal structure of the amplitude envelope of the waves, $A(x, t)$. We focused our analysis on the amplitude envelope after the waves reached quasi-steady state in the measurement window. The time to reach this state was approximately the time for waves to propagate at the group velocity from the wave maker to the end of the measurement zone. While in quasi-steady state, the amplitude envelope varied little in time but decayed spatially. We denote these measurements by $\bar{A}(x)$.

Particularly for experiments in which $\bar{A}(x)$ decreased significantly over the measurement window, we characterized the wave attenuation by the decay distance, $\sigma_{1/2}$, which measures the distance over which the wave amplitude decays to half its original value. When measuring this distance from the wave-gauge data, the start of the amplitude decay was taken to be at the location of the first wave-gauge and interpolation was used to determine $\sigma_{1/2}$. If the wave amplitude visibly decayed but did not drop below half its original value over the measurement window, an exponential curve was fit to the data with this curve being extrapolated to determine $\sigma_{1/2}$. For a single experiment, the decay distance was computed at 5 different times taken 5 seconds apart after the waves first reached quasi-steady state. From these measurements we computed both the mean and standard deviation of $\sigma_{1/2}$. For weakly attenuated waves measured by wave-gauge data, the error in $\sigma_{1/2}$ was taken from the error associated with extrapolating data, this being larger than the error from variation in time.

Results

First, we present results that examine the dependence of wave attenuation upon wave frequency and amplitude as waves pass under a close-packed layer of spheres. We then examine how the area concentration of spheres influences the attenuation of waves incident with a fixed frequency and amplitude.

Wave attenuation by close-packed spheres

The measurements of amplitude, $\bar{A}(x)$, from wave gauges in six experiments with incident wave frequencies ranging from $f = 1.0$ Hz to 2.0 Hz and fixed relative amplitude $\epsilon = ka_0 = 0.20$ are plotted in Fig. 5. This shows

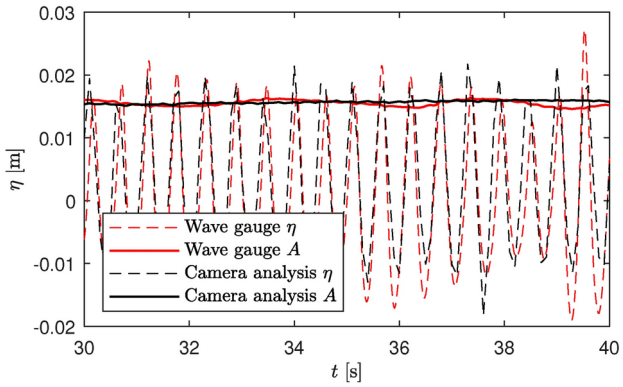

Figure 4. Comparison of the free surface displacement, η (dashed lines), and amplitude, A, (solid lines) measured by a wave gauge at $x = 12.50$ m from the wave maker (red) and at the same location as recorded by a side camera (black).

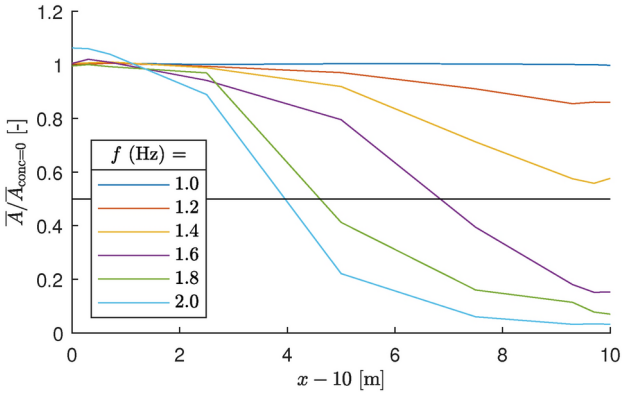

Figure 5. Relative amplitude versus distance across the observation window measured by wave gauges in experiments with fixed steepness $\epsilon \equiv ka_0 = 0.20$ and different incident wave frequencies, as indicated in the legend. The amplitude $\bar{A}(x)$ is normalized by the amplitude $\bar{A}_{\mathrm{conc}=0}$ measured in experiments with the same forcing amplitude and frequency, but no floating spheres.

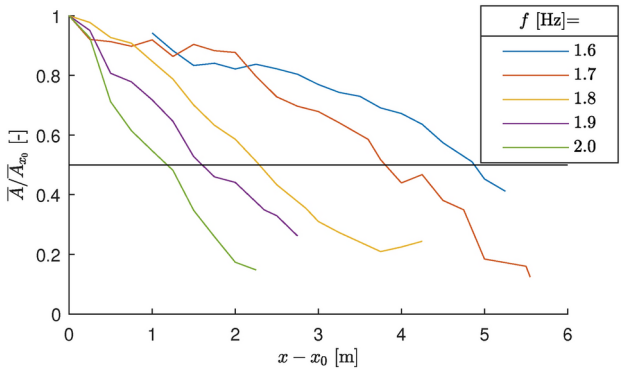

Figure 6. As in Fig. 5, but showing relative amplitude versus downstream distance as measured by side cameras in experiments with relatively high-frequency incident waves and $\epsilon = 0.25$. Here downstream distance is measured with respect to the location, x_0, at which the wave decay begins, and amplitude is normalised by the amplitude at this location, $\bar{A}_{x_0}$. Where the black horizontal line crosses each curve gives the decay distance, $\sigma_{1/2}$.

a strong dependence of wave attenuation upon incident wave frequency with little attenuation occurring for a 1.0 Hz incident wave to halving the amplitude of the incoming wave over $\simeq 4$ m for a 2.0 Hz wave.

When the spatial damping was on the scale of a few meters (for $f \geq 1.6$ Hz), the side cameras more accurately measured the spatial attenuation of the waves. Their results, from experiments with $\epsilon = 0.25$, are shown in Fig. 6.

Amplitude decay distances, $\sigma_{1/2}$, were calculated from measurements of amplitude envelope versus downstream distance, as determined by wave-gauge data (e.g. Fig. 5) and the side cameras (e.g. Fig. 6). The results from all experiments are shown in Fig. 7. The error bars are associated with the accuracy of measuring the surface displacement, which gives larger errors for smaller amplitude waves. In experiments for which the amplitude decayed by half over a distance of a few meters ($f \gtrsim 1.6$ Hz), the error in coarse spatial resolution wave gauge data was comparable to $\sigma_{1/2}$, and so these points are excluded. Fig. 7 shows a rapid decrease in the decay distance with increasing frequency and incident wave amplitude.

Effect of reducing concentration

We also performed experiments in which the initial area concentration of spheres was not 100% (for close-packed spheres). The spatial decay of amplitude measured in experiments with fixed wave steepness and frequency, but varying concentration, are shown in Fig. 8. This shows that the waves attenuated negligibly if the area concentration was smaller than $\simeq 57\%$. At larger concentrations, the horizontally convergent flow near wave crests resulted in the spheres becoming close-packed. Using wave-gauge data, the measured values of $\sigma_{1/2}$ for experiments with waves forced at frequency 1.8 Hz and steepness $\epsilon = 0.20$ are 12 (± 2) m for a concentration of 71%, 5.8 (± 0.7) m for a concentration of 86%, and 4.2 (± 0.4) m for a concentration of 100% (Fig. 1 in the Supplementary Information shows $\sigma_{1/2}$ as a function of area concentration; it is not straightforward to directly determine the functional dependence on concentration from this data). For completeness, we note that the small increase in amplitude that can be observed for small x for area concentrations of 28-86% is likely caused by a

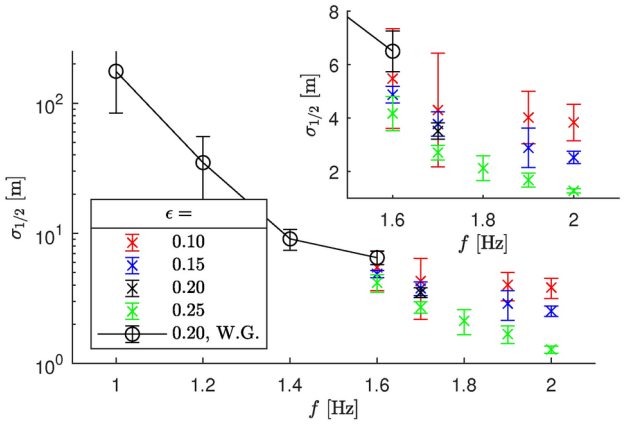

Figure 7. Spatial decay distance $\sigma_{1/2}$ with errors estimated for all experiments as a function of wave frequency f [Hz] for different values of steepness ϵ, as denoted by the legend. The black line with open circle markers are from wave gauge measurements. The rest are based on measurements using cameras.

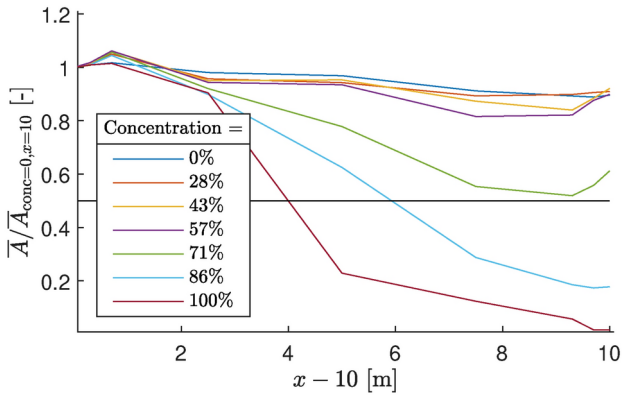

Figure 8. As in Fig. 5, but showing relative amplitude versus distance in experiments with fixed steepness $\epsilon \equiv ka_0 = 0.20$ and frequency $f = 1.8$ Hz and different area concentrations of particles, as indicated in the legend.

calibration error of a single gauge; this does not affect our estimates of the decay distances $\sigma_{1/2}$ resulting from these data.

Theoretical estimates of the order-of-magnitude of damping

Here, we use theoretical arguments to estimate length scales associated with wave attenuation due to viscosity and the presence of floating particles and compare these to our measurements. The waves are assumed to lie on the surface of deep water, satisfying the dispersion relation

$$\omega^2 = gk, \tag{1}$$

in which k is the wavenumber, g is gravity, and ω is the frequency in radians per second. (For the purpose of theory, it is convenient to use ω instead of the frequency in Hz, $f = \omega/(2\pi)$.) The spatio-temporal evolution of the horizontal velocity associated with the waves is represented by

$$u(x, z, t) = A(x)\,\omega\, e^{kz} \cos(kx - \omega t), \tag{2}$$

in which the undisturbed surface is at $z = 0$, and A is the amplitude envelope of the surface displacement, which decreases with downstream distance x as a consequence of wave attenuation. The phase of the wave is arbitrarily set so that the wave is at its maximum amplitude, A_0, at $x = 0$ and $t = 0$. The amplitude envelope is assumed to vary slowly in space compared with the horizontal wavelength of the waves so that the waves can be treated locally as being horizontally periodic and satisfying the dispersion relationship (1). That is, the waves are quasi-monochromatic.

From the polarization relation of deep-water waves, the mean horizontal flux of energy per unit width and mass is given by

$$F = \langle up \rangle = \frac{1}{4}\frac{\omega^3}{k^2}A^2 = \frac{1}{4}\frac{g^2}{\omega}A^2. \tag{3}$$

Here p is pressure per mass, which is related to u for small-amplitude waves by $p = c_p u$, with $c_p = \omega/k$ being the horizontal phase speed. The angle brackets denote averaging over one period in time. In the last expression, we have used the dispersion relation (1).

In steady state, the energy flux (and hence the wave amplitude) decreases with downstream distance as a consequence of energy dissipation due to laminar or turbulence-enhanced viscous processes. Generally, the total mechanical energy balance is represented by

$$\frac{dF}{dx} = -\mathscr{E}, \tag{4}$$

in which $\mathscr{E}$ is the energy dissipation per width and mass. Expecting that $\mathscr{E}$ depends on the amplitude A, equations (4) and (3) give a differential equation for A that can be solved to determine how A varies with x and so determine the decay distance, σ.

Various processes can result in energy dissipation. We neglect the influence of viscosity within the bulk of the fluid and acting along the side walls of the tank, as these clearly act negligibly to attenuate the waves in the absence of particles (though see Sutherland & Balmforth[19]). Previous work[23] calculated the inertial motion associated with an isolated buoyant sphere at the surface of waves, with the sphere moving differentially with respect to the fluid at the surface. From that work, dissipation associated with motion around a single sphere can be computed, summed over all particles over the tank width, and then dividing by width to estimate $\mathscr{E}$. This calculation predicts decay distances much larger than decay distances resulting from sidewall viscous dissipation, as might be anticipated from the smaller relative velocities and surface areas involved, as well as from experiments showing little attenuation occurring if the area concentration of particles is below $\simeq 57\%$.

Because experiments show that the close-packing of spheres has a strong influence upon wave attenuation, below we consider processes whereby energy is lost as a consequence of waves passing below a close-packing of floating spheres.

Dissipation below an inextensible thin sheet (no-slip)

Here we treat the floating particles as being everywhere close-packed, acting like an inextensible thin surface sheet that does not inhibit vertical motion but provides a no-slip upper boundary to the horizontal motion associated with the waves. This is a well-studied model for the attenuation of waves in the Arctic Ocean by sea ice[12,18]. The inextensible sheet creates a boundary layer with additional vorticity due to the no-slip condition and thus damping the sheet provides compared to a free surface. The depth of the oscillatory boundary layer below the sheet is given by[12,24]

$$\delta = \sqrt{2\nu/\omega}, \tag{5}$$

where ν is the kinematic viscosity. The energy dissipation rate per width and mass is found using the positive definite form of the dissipation involving squared components of the rate of strain tensor (cf. Lamb[24], Art 329, eq. 8). Assuming $k\delta \ll 1$ and that the dissipation is equivalent to that for motion below an oscillating plate, with analytic solution $u = A\omega \exp(z/\delta)\cos(z/\delta + \omega t)$, we find (after averaging over one wave period) the following:

$$\mathscr{E}_e \sim \nu(A\omega)^2/(2\delta). \tag{6}$$

Substituting this for $\mathscr{E}$ in (4), and using (3) gives

$$\frac{dA^2}{dx} = -\frac{2}{\sigma_\delta}A^2, \quad \text{with} \quad \sigma_\delta = 2^{1/2}\frac{g^2}{(\nu\omega^7)^{1/2}}. \tag{7}$$

Solving this equation shows that A decays exponentially with distance over an e-folding decay distance σ_δ: $A(x) = A_0 \exp(-x/\sigma_\delta)$. An equivalent expression for the spatial damping was found by Sutherland et al.[12]

Values of σ_δ for various frequencies corresponding to those in our experiments are given in Table 1. These show a significant decrease in the spatial decay distance with increasing frequency, but being independent of amplitude. The distance, $\sigma_{1/2}$, for the amplitude to decay by half (as measured in experiments) is obtained by multiplying σ_δ by $\ln(2) \simeq 0.69$. These distances are comparable to those measured in experiments with frequencies between 1.6 and 2.0 Hz.

ω	1.0 Hz $\simeq$ 6.3 rad/s	1.6 Hz $\simeq$ 10.1 rad/s	2.0 Hz $\simeq$ 12.6 rad/s
$\sigma_\delta \ \ln(2)$ [m]	150	29.4	13.8
$\sigma_R \ \ln(2)$ [m]	1342	328	168
σ_t [m]	7.9	3.1	2.0

Table 1. Predicted amplitude decay distances for different dissipation models: e-folding scales σ_δ (7) and σ_R (8) due to dissipation below an inextensible thin sheet (no-slip) assuming a viscous and a rough boundary layer respectively, and the half-amplitude scale σ_t (10) due to dissipation due of turbulent flow below spheres. The e-folding scales are multiplied by $\ln(2)$ to give the corresponding half-amplitude scale, so they can be compared directly with σ_6 and the values of $\sigma_{1/2}$ obtained from experiments. For σ_R, we set $R = 1$ cm. For σ_t we set $\epsilon = 0.2$ and $C = 12.8$

Although this agreement may be considered acceptable given the approximations leading to (6), it is unlikely that the inextensible thin sheet model captures the essential physics. This is because the oscillatory boundary layer depth, δ, is much smaller than the size of the spheres. For example, taking $\omega = 12.6$ rad /s ($f = 2.0$ Hz), (5) gives $\delta \simeq 0.03$ cm, which is much smaller than the $R = 1$ cm radius of the floating spheres. If we suppose dissipation occurs on a scale R instead of δ, the vertially integrated dissipation rate is of the order $\nu(A\omega)^2/R$. Hence the estimated e-folding decay distance is

$$\sigma_R \sim \frac{R}{2}\frac{g^2}{\nu\omega^3}. \tag{8}$$

These values, given in Table 1, are much larger than σ_δ for a given frequency, and orders of magnitude larger than what is observed in experiments.

Dissipation due to turbulent flow below spheres

Given the relatively small viscous boundary layer depth, δ, compared with the sphere radius, R, (which may be considered as a roughness scale), it is reasonable to suppose the flow under close-packed spheres is turbulent. Indeed the Reynolds number for flow over a sphere based on the flow speed, $A_0\omega$, and radius, R, is $\mathrm{Re} = A_0R/\delta^2$, which is on the order 1000 for $R = 1$ cm, $A_0 \sim 1$ cm, and $\omega \simeq 12.6$ rad /s ($f = 2.0$ Hz).

We estimate the energy dissipation rate due to turbulent flow over the spheres by assuming that wave energy, which scales as $(A\omega)^2$, is injected into turbulence on the time scale for flow under a sphere, which scales as $R/(A\omega)$, and that turbulent dissipation occurs over a depth R. Hence the turbulent energy dissipation rate per width and mass below close-packed spheres is estimated by

$$\mathscr{E}_t = C(A\omega)^3, \tag{9}$$

in which the non-dimensional constant C is a measure of conversion from turbulent power production to dissipation. A similar scaling was found in studies of steady turbulent flow over rough boundaries[25]. Therein the energy dissipation rate was found to scale as u_τ^3, in which u_τ is the friction velocity, which itself is proportional to the velocity far from the boundary[26].

Substituting (9) for $\mathscr{E}$ in (4), and using (3) gives $dA^2/dx \sim -4k^2A^3$, which has a non-exponential solution:

$$A(x) = A_0/(1 + x/\sigma_t), \quad \text{with} \quad \sigma_t = g/(2C\epsilon\omega^2), \tag{10}$$

in which $\epsilon = A_0k$ is the initial wave steepness. Here σ_t represents the distance over which the amplitude of the wave drops by half. Using the dispersion relation (1), we see that the scaled decay distance is $k\sigma_t = 1/(2C\epsilon)$, which depends only upon wave steepness for given conversion constant, C. This collapse of data is shown in Fig. 9.

We empirically estimate the value of C by finding values of $1/(2\epsilon k\sigma_{1/2})$ measured in each of our experiments with $f = 1.6$ to 2.0 Hz (for which significant amplitude decay was observed). Thus we find $C = 0.078 \pm 0.011$.

Finally, we estimate wave attenuation when passing through floating spheres that are not close-packed. Suppose the mean separation distance in x between the centres of neighbouring undisturbed spheres is $2R + \Delta_0$. Assuming the spheres are non-inertial and neglecting the Stokes drift, the wave horizontally displaces a sphere initially at x by a distance $-A\sin(kx)$, in which $x = 0$ corresponds to a wave crest. Consider a pair of neighbouring spheres whose centres are separated by a distance $2R + \Delta_0$ before the wave arrives, being located at $x + (2R + \Delta_0)/2$ and $x - (2R + \Delta_0)/2$. After the wave arrives, they are separated by

$$\Delta(x) \simeq 2R + \Delta_0 - Ak\cos(kx)(2R + \Delta_0), \tag{11}$$

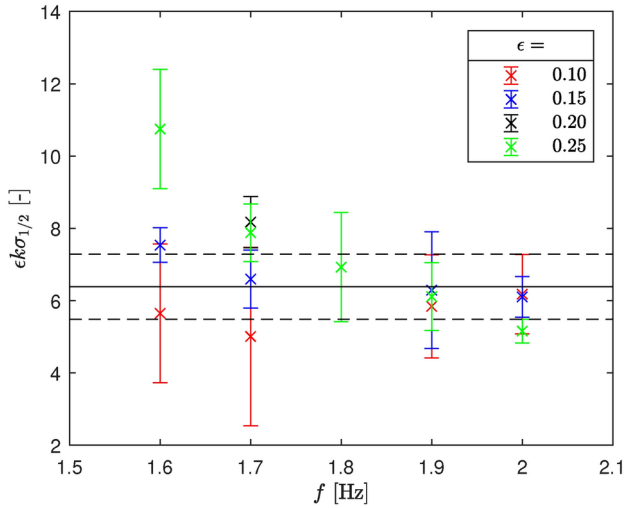

Figure 9. Data in Fig. 7 replotted as $\epsilon k\sigma_{1/2}$ versus frequency. The horizontal solid and dashed black lines indicate the best-fit mean and standard deviation of the non-dimensional constant $1/(2C) = 6.4 \pm 0.9$.

in which we have assumed the waves are long compared to the separation distance so that $k(2R + \Delta_0) \ll 1$. Spheres will only be brought into contact if $\Delta(x) \leq 2R$. This occurs only if $\Delta_0 \leq \Delta_c$, in which

$$\Delta_c \equiv 2R\frac{\epsilon}{1-\epsilon}, \tag{12}$$

in which $\epsilon = Ak$ is the wave steepness.

At an incident wave steepness of $\epsilon = 0.2$, for example, we predict that close-packing will occur near the wave crest only if the initial separation between adjacent spheres has $\Delta_0 \leq 0.5R$. This corresponds approximately to an area concentration greater than $\sim 50\%$, consistent with our experiments that show significant damping is only beginning to occur for area concentrations above $\sim 60\%$ (cf. Fig. 6).

Discussion and conclusions

We performed laboratory experiments to investigate the damping of progressive deep-water waves by a monolayer of floating spheres. The presence of spheres had no discernible influence upon wave attenuation unless the area concentration of spheres was high ($\gtrsim 71\%$ of being close-packed) and the frequency was sufficiently large (above 1.5 Hz). However, if the spheres were close-packed and the wave frequency sufficiently large, the waves were found to attenuate over a remarkably short distance, on the order of a few meters.

While the rapid attenuation of the waves is predicted reasonably well by an inextensible thin-sheet model, typically used to predict the attenuation of ocean waves by sea ice, similarly to Squire[18] and Herman[27] for sea ice, we argue that exponential decay does not correctly capture the physics of wave damping by floating spheres in part because the predicted viscous boundary layer thickness is much smaller than the size of the spheres and the decay distance is independent of amplitude. Using an inextensible thin sheet-sheet model with the sphere radius instead of the viscous boundary layer depth overpredicts the decay distance by two orders of magnitude. Also, because the Reynolds number associated with flow passing under the spheres is on the order of 1000, we argue that the oscillatory flow due to waves over the underside of the spheres is turbulent. We developed a theory for the spatial attenuation of waves accounting for power lost to turbulence. This predicts a power law, rather than exponential decay. Using an empirical parameter that represents the fraction of power injected into turbulence that ultimately is dissipated, we predict reasonable values for the attenuation distance which depends on the incident wave frequency ($1.0 < f < 2.0$ Hz for a sphere diameter $D = 20$ mm) and steepness ($0.1 < ak < 0.25$). If floating spheres become close-packed, which occurs at concentrations greater than 50-60%, wavelengths from approximately 25 times the sphere diameter become damped within a few wavelengths, and this distance is shorter for steeper waves.

This work may provide new insights into wave attenuation by pancake sea ice, particularly in the marginal ice zone of the Southern Ocean. Hopefully, this work will give a better understanding of the different physics involved in various types of ice floes as highlighted by Squire[18]. In the context of sea ice, others have also argued for non-exponential wave attenuation.[18] Herman[27] reviewed previous studies of wave attenuation in sea ice and questions the assumption that wave decay is exponential, stating that only very few studies carry out a least-squares fit or investigate other functional forms. Some studies have found non-exponential decay under sea ice. Kohout et al.[8] observed an almost linear decay of large waves under sea ice in the Ross and Amundsen-Bellingshausen seas. Montiel et al.[9] predominantly measured exponential decay in data from wave buoys measuring during a three-day storm in the Beaufort Sea but found that a linear decay fitted some results more accurately. Herman

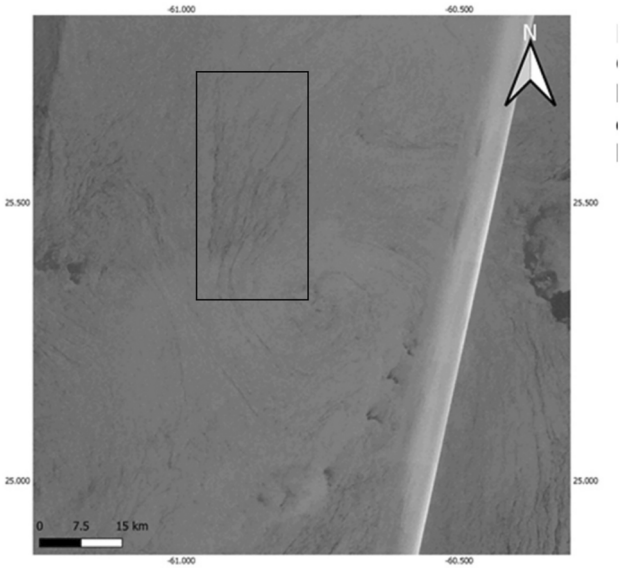

Figure 10. SAR image of the Atlantic Ocean taken by Sentinel-1 on 10th June 2014 showing dark bands (inside the box), which may show the presence of plastic because these bands cannot be explained by either ice, algae blooms, or oil (which are normally attributed to such results). [Image provided courtesy of the European Space Agency (ESA).].

et al[28,29] numerically modeled ice floes using a discrete-element model to investigate how ice-water drag caused wave decay and found that waves decay according to a non-exponential relationship $a(x) = 1/(\alpha x + 1/a_0))$, similar to the relationship identified in the present paper, and compared with experimental results. Brouwer et al[30] used satellite data to measure wave propagation into the marginal ice zone and found that fitting a linear model resulted lower error than the often assumed exponential decay.

Originally motivating this work was the question if floating plastic waste in the ocean could be detected by satellite. Previously satellites using synthetic aperture radar (SAR) have, for example, detected oil slicks on the ocean as a consequence of the oil attenuating waves, reducing the scattering of incident light radiation and resulting in dark bands in SAR images[31]. Because most floating plastics in the ocean have low area concentrations, our work suggests that they would negligibly influence wave attenuation and could not be detected by SAR. However, some SAR imagery, such at that shown in Fig. 10, reveal dark bands that cannot be explained by factors such as oil slicks. Submesoscale ocean dynamics are known to accumulate drifting particles at surface convergent fronts or windrows by thousands of times their undisturbed concentrations[32,33]. And so it could be that floating plastics that converge due to such processes could result in wave attenuation and consequent detection by satellite. Such dynamics remain to be investigated.

Data availibility

The datasets generated during and/or analysed during the current study are available from the corresponding author on reasonable request.

Received: 7 March 2024; Accepted: 8 January 2025
Published online: 13 January 2025

References

1. Hoult, D. P. Oil spreading on the sea. *Ann. Rev. Fluid Mech.* **4**, 341–368 (1972).
2. Viola, F., Brun, P.-T., Dollet, B. & Gallaire, F. Foam on troubled water: Capillary induced finite-time arrest of sloshing waves. *Phys. Fluids* **28**, 091701 (2016).
3. Viola, F. & Gallaire, F. A theoretical framework to analyze the combined effect of surface tension and viscosity on the damping rate of sloshing waves. *Phys. Rev. Fluids* **3**, 094801 (2018).
4. Squire, V. A. Ocean wave interactions with sea ice: A reappraisal. *Annu. Rev. Fluid Mech.* **52**, 37–60 (2020).
5. Bennetts, L. G. & Williams, T. D. Water wave transmission by an array of floating discs. *Proc. R. Soc. A. Math. Phys.* **471**, 20140698 (2015).
6. Alberello, A. et al. A physical model of wave attenuation in pancake ice. *Int. J. Offshore Polar* **31**, 263–269 (2021).
7. Passerotti, G. et al. Interactions between irregular wave fields and sea ice: A physical model for wave attenuation and ice breakup in an ice tank. *J. Phys. Oceanogr.* **52**, 1431–1446 (2022).
8. Kohout, A. L., Williams, M., Dean, S. & Meylan, M. Storm-induced sea-ice breakup and the implications for ice extent. *Nature* **509**, 604–607 (2014).
9. Montiel, F., Squire, V., Doble, M., Thomson, J. & Wadhams, P. Attenuation and directional spreading of ocean waves during a storm event in the autumn beaufort sea marginal ice zone. *J. Geophys. Res.-Oceans* **123**, 5912–5932 (2018).
10. Toffoli, A. et al. Sea ice floes dissipate the energy of steep ocean waves. *Geophys. Res. Lett.* **42**, 8547–8554 (2015).
11. Montiel, F., Squire, V. A. & Bennetts, L. G. Attenuation and directional spreading of ocean wave spectra in the marginal ice zone. *J. Fluid Mech.* **790**, 492–522 (2016).

12. Sutherland, G., Halsne, T., Rabault, J. & Jensen, A. The attenuation of monochromatic surface waves due to the presence of an inextensible cover. *Wave Motion* **68**, 88–96 (2017).
13. Newyear, K. & Martin, S. A comparison of theory and laboratory measurements of wave propagation and attenuation in grease ice. *J. Geophys. Res.-Oceans* **102**, 25091–25099 (1997).
14. Keller, J. B. Gravity waves on ice-covered water. *J. Geophys. Res.-Oceans***103**, 7663–7669 (1998).
15. Balmforth, N. & Craster, R. Ocean waves and ice sheets. *J. Fluid Mech.* **395**, 89–124 (1999).
16. Mosig, J. E. M., Montiel, F. & Squire, V. A. Comparison of viscoelastic-type models for ocean wave attenuation in ice-covered seas. *J. Geophys. Res.-Oceans* **120**, 6072–6090 (2015).
17. Shen, H. H. & Squire, V. A. *Wave Damping in Compact Pancake Ice Fields Due to Interactions Between Pancakes*, 325–341 (AGU, 1998).
18. Squire, V. A. A fresh look at how ocean waves and sea ice interact. *Philos. Trans. R. Soc. A* **376**, 20170342 (2018).
19. Sutherland, B. R. & Balmforth, N. J. Damping of surface waves by floating particles. *Phys. Rev. Fluids* **4**, 014804 (2019).
20. Gurusamy, S., Meylan, M. H., Kumar, D. & Patnaik, B. Frequency dependent decay of water waves due to floating balls with application to simulating wave decay in the marginal ice zone. *J. Fluids Struct.* **117**, 103817 (2023).
21. Sun, Y., Bakker, T., Ruf, C. & Pan, Y. Effects of microplastics and surfactants on surface roughness of water waves. *Sci. Rep.* **13**, 1978 (2023).
22. Montiel, F. *et al.* Hydroelastic response of floating elastic discs to regular waves. Part 1. wave basin experiments. *J. Fluid. Mech.* **723** (2013).
23. Calvert, R. et al. A mechanism for the increased wave-induced drift of floating marine litter. *J. Fluid Mech.* **925**, A73 (2021).
24. Lamb, H. *Hydrodynamics* (Cambridge University Press, Cambridge, 1932), 6 edn.
25. Kadivar, M., Tormey, D. & McGranaghan, G. A review on turbulent flow over rough surfaces: Fundamentals and theories. *Int. J. Thermofluids* **10**, 100077 (2021).
26. Kim, T., Blios, G., Best, J. L. & Christensen, K. T. PIV measurements of turbulent flow overlying large, cubic- and hexagonally-packed hemisphere arrays. *J. Hydraul. Res.* **58**, 363–383 (2020).
27. Herman, A. From apparent attenuation towards physics-based source terms—A perspective on spectral wave modeling in ice-covered seas. *Front. Mar. Sci.* **11**, 1413116 (2024).
28. Herman, A., Cheng, S. & Shen, H. H. Wave energy attenuation in fields of colliding ice floes-part 1: Discrete-element modelling of dissipation due to ice-water drag. *Cryosphere* **13**, 2887–2900 (2019).
29. Herman, A., Cheng, S. & Shen, H. H. Wave energy attenuation in fields of colliding ice floes-part 2: A laboratory case study. *Cryosphere* **13**, 2901–2914 (2019).
30. Brouwer, J. et al. Altimetric observation of wave attenuation through the antarctic marginal ice zone using ICESat-2. *Cryosphere* **16**, 2325–2353 (2022).
31. Wiley, C. A. Synthetic aperture radars. *IEEE Trans. Aerosp. Electr. Syst.* 440–443 (1985).
32. D'Asaro, E. A. et al. Ocean convergence and the dispersion of flotsam. *Proc. Natl. Acad. Sci.* **115**, 1162–1167 (2018).
33. Cózar, A. *et al.* Marine litter windrows: A strategic target to understand and manage the ocean plastic pollution. *Front. Mar. Sci.* **8** (2021).

Acknowledgements

This research was performed through funding by the European Space Agency (Grant No. 4000136626/21/NL/GLC/my). We would like to thank Pieter van der Gaag, Chantal Willems, Arie van der Vlies and Arno Doorn at Delft University of Technology for their help setting up and conducting the experiments.

Author contributions

B.S. and T.v.d.B. conceived the experiments. R.S. and J.M. conducted the experiments. R.S. and B.S. analyzed the results. All authors contributed to writing, editing and reviewing the manuscript.

Funding

This research was performed through funding by the European Space Agency (Grant No. 4000136626/21/NL/GLC/my).

Declarations

Competing interests

The authors declare no competing interests.

Additional information

Supplementary Information The online version contains supplementary material available at https://doi.org/10.1038/s41598-025-86142-4.

Correspondence and requests for materials should be addressed to T.S.B.